Title

In Vivo Tracking of Copper-64 Radiolabeled Nanoparticles in Lactuca sativa.

Journal

Environmental science & technology, 51(21)

ISSN

0013-936X

Authors

Davis, Ryan A
Rippner, Devin A
Hausner, Sven H
et al.

Publication Date

2017-11-01

DOI

10.1021/acs.est.7b03333

Peer reviewed

Environmental Science & Technology

Article

Cite This: Environ. Sci. Technol. XXXX, XXX, XXX-XXX

pubs.acs.org/est

In Vivo Tracking of Copper-64 Radiolabeled Nanoparticles in *Lactuca sativa*

Ryan A. Davis,[†,‡] Devin A. Rippner,[§] Sven H. Hausner,[†,‡] Sanjai J. Parikh,[§] Andrew J. McElrone,[∥] and Julie L. Sutcliffe*[,†,‡,⊥,#]

[†]Department of Internal Medicine, Division of Hematology & Oncology, [‡]Radiochemistry Research and Training Facility, [§]Department of Land, Air and Water Resources, [∥]USDA-ARS, Department of Viticulture and Enology, [⊥]Department of Biomedical Engineering, and [#]Center for Molecular and Genomic Imaging, University of California—Davis, 2921 Stockton Blvd, Sacramento, California 95817, United States

Supporting Information

ABSTRACT: Engineered nanoparticles (NPs) are increasingly used in commercial products including automotive lubricants, clothing, deodorants, sunscreens, and cosmetics and can potentially accumulate in our food supply. Given their size it is difficult to detect and visualize the presence of NPs in environmental samples, including crop plants. New analytical tools are needed to fill the void for detection and visualization of NPs in complex biological and environmental matrices. We aimed to determine whether radiolabeled NPs could be used as a noninvasive, highly sensitive analytical tool to quantitatively track and visualize NP transport and accumulation in vivo in lettuce (*Lactuca sativa*) and to investigate the effect of NP size on transport and distribution over time using a combination of autoradiography, positron emission tomography (PET)/computed tomography (CT), scanning electron microscopy (SEM), and transition electron microscopy (TEM). Azide functionalized NPs were radiolabeled via a "click" reaction with copper-64 (^{64}Cu)-1,4,7-triazacyclononane triacetic acid (NOTA) azadibenzocyclooctyne (ADIBO) conjugate ([^{64}Cu]-ADIBO-NOTA) via copper-free Huisgen-1,3-dipolar cycloaddition reaction. This yielded radiolabeled [^{64}Cu]-NPs of uniform shape and size with a high radiochemical purity (>99%), specific activity of 2.2 mCi/mg of NP, and high stability (i.e., no detectable dissolution) over 24 h across a pH range of 5−9. Both PET/CT and autoradiography showed that [^{64}Cu]-NPs entered the lettuce seedling roots and were rapidly transported to the cotyledons with the majority of the accumulation inside the roots. Uptake and transport of intact NPs was size-dependent, and in combination with the accumulation within the roots suggests a filtering effect of the plant cell walls at various points along the water transport pathway.

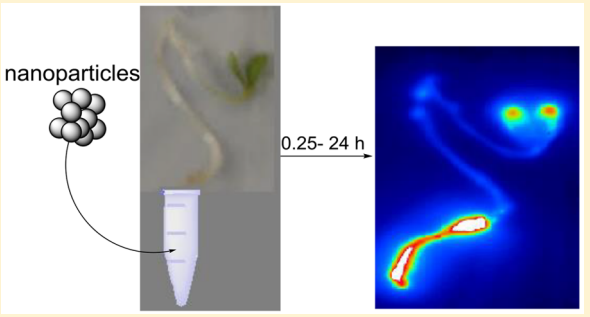

INTRODUCTION

The increasing use of NPs in commercial products has led to NP-accumulation in the environment and within the food chain.[1−9] Chronic exposure to NPs can lead to health issues as some inorganic NPs have biological activity at the cellular and subcellular level with an unknown cytotoxicity and genotoxicity.[3,4,10] In particular, metal oxide NPs are the most abundant form of NP in the environment with the most potential toxic risks.[7,11] Locating, quantifying, and imaging NPs in vivo can provide information on biodistribution and fate of NPs in living systems.[12,13] However, many challenges to quantitatively assess their biodistributions under realistic environmental exposure concentrations (mg L^{-1} to ng L^{-1}) remain.[5]

To date, the visualization of most NPs within plants has relied on the use of micro-X-ray fluorescence spectrometry (μ-XRF), confocal microscopy, TEM, SEM, scanning transmission electron microscopy (STEM), or scanning transmission ion microscopy (STIM).[14−20] The most prominent quantification techniques have been inductively coupled plasma spectroscopy (ICP) utilizing either optically emission spectroscopy (OES) or mass spectrometry (MS).[1,14−20] In a few cases atomic absorption spectroscopy (AAS) has been used for quantification.[21] These techniques required mineralization of the plant material generally with hydrogen peroxide and nitric acid, and may not be sufficiently sensitive enough to quantify small changes in the amount of a metal ion.[1,22,23] Notably, high background concentrations of essential nutrients make detecting and quantifying the small variation in NP-related metal ion content an analytical challenge as the measurement is often of the same magnitude as noise or at the detection limit.[1,22,23] Optically tagged NPs have also been investigated, but the challenge of overcoming the plants' own bioluminescence can make quantification difficult.[24,25]

Although used in medical imaging, radiolabeled NPs for noninvasive tracking and quantification in plants have not been

Received: July 3, 2017
Revised: September 11, 2017
Accepted: September 27, 2017
Published: September 27, 2017

DOI: 10.1021/acs.est.7b03333
Environ. Sci. Technol. XXXX, XXX, XXX−XXX

significantly explored.[12,13] Prior radiolabeling of NPs for medical imaging has utilized three main approaches: (1) postradiolabeling via attachment of chelator to NPs first, then reaction with the a metal radionuclide; (2) preradiolabeling, where a radioactive prosthetic group, a small molecule that the radioisotope is attached, followed by attachment to the NP; and (3) direct radiolabeling.[13] Of these three main radiolabeling approaches, the third approach has been the only method used to study NP distribution in plants where Zhang et al.[12] reported the use of [^{141}Ce]CeO_2-NPs produced via neutron bombardment of CeO_2-NPs to study distribution in cucumbers. The produced radionuclide ^{141}Ce has a 32.51 day half-life, and the specific activity of the synthesized [^{141}Ce]CeO_2-NPs was 2.7 μCi/mg of NP.[12]

Despite numerous approaches to analyze NPs, a combination of technologies is required due to the low detection limits (ppb-ppt) and high resolution (nm) needed to address the intact nature of NP-transport into plants. Thus, multiple tools must be utilized to quantify and determine the intact nature of NPs at a given location within biological environments (Figure 1).[26] Previous studies have provided conflicting evidence about

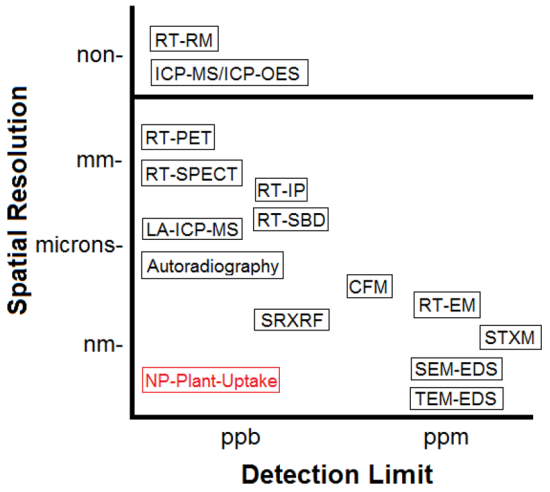

Figure 1. Spatial and quantitative limits of instruments used to identify nanoparticles (Figure adapted from ref 26). Black boxes indicate the analytical method/instrumentation. The red box shows the range of detection and spatial resolution required to quantify and visualize NPs within plants. Abbreviations: RT-radiotracing, RM-radiometry, SPECT-single photon emission computed tomography, IP-imaging plate, SBD-silicon based detector, LA-laser ablation, CFM-confocal fluorescence microscopy, EM-electron microscopy, SRXRF-synchrotron radiation micro-X-ray fluorescence, EDS-energy dispersive x-ray spectroscopy, and STXM-scanning transmission X-ray microscopy. Instruments at top do not have spatial resolution (RT-RM and ICP).

the intact nature of NP uptake and transport into plants: some studies indicated intact NP uptake and vascular transport,[10,12,15,16,20,27−32] some observed NPs in plants due to dissolution events and reformation within the plant tissue,[14,17−19,33−35] and still others have indicated that NPs cannot be transported into plants.[22,36−38] These varied observations could be linked to inadequate techniques available to track NP movement in vivo. The main challenge in determining intact NP transport into plants is ruling out NP-dissolution, as reductive precipitation and formation of NPs within plant tissue has been documented.[39−43] Even natural formation of NPs within plants and fungi is known.[44] Further complicating the picture is the fact that many studies assessing NP uptake exposed plants over long periods of time from 2 to 130 days, with very large amounts of NPs (500−10 000 mg L^{-1}) per plant, which could make dissolution events more prevalent.[1,10,16−32,36,45] Avoiding excessive exposure to the NPs (both, in concentration and time) and carefully analyzing the stability of the administered NPs are key to avoid erroneous conclusions due to NP-dissolution and subsequent reformation.

In this study we evaluated an analytical method using a radioactive label to noninvasively track and quantify transport and accumulation of NPs in lettuce seedlings in vivo. This method studied NP-size dependent transport immediately upon exposure (<1 day), an early time frame that has rarely been explored in plants.[31] The visualization of NP transport and accumulation in lettuce seedlings was done by autoradiography and PET/CT imaging and further confirmed by gamma-counting, SEM, and TEM. Our study was designed to use highly uniform NPs (shape and size) of two size sets (10 and 20 nm), which were theoretically too large for passive transport across plant tissues (pore size ≤2 nm).[6,7] To ensure a narrow size distribution with a uniform geometric shape and the ability to thoroughly investigate stability (i.e., no dissolution and reprecipitation inside the plant), a preradiolabeling method with the PET-radioisotope copper-64, the "clickable" chelator ADIBO-NOTA, and commercially available spherical Fe_3O_4-NPs containing azides was explored. This radiolabeling approach yielded a high specific activity (mCi/mg of NP) and allowed for size characterization of the NPs after the plant accumulation and imaging period, and avoided complication from fabricating radioactive NPs and production of less stable NP material with a larger size distribution. Rigorous stability studies were carried out at a variety of pHs to investigate possible dissolution of the ^{64}Cu-radiolabeled NPs and substantiate the intact nature of NP-transport into lettuce seedlings.

MATERIALS AND METHODS

Hydroponic Culture. Lettuce (*Lactuca sativa* "Green Towers") seeds were germinated at 25 °C in Petri dishes hydroponically in Hoagland's solution containing: 210 mg L^{-1} of nitrogen, 235 mg L^{-1} of potassium, 200 mg L^{-1} calcium, 31 mg L^{-1} phosphorus, 64 mg L^{-1} sulfur, 48 mg L^{-1} magnesium, 0.5 mg L^{-1} boron, 1.35 mg L^{-1} iron, 0.5 mg L^{-1} manganese, 0.05 mg L^{-1} zinc, 0.02 mg L^{-1} copper, and 0.01 mg L^{-1} molybdenum. Seedlings were grown in the dark for 7 days and then transferred to constant light for 2 days prior to use in the experiment. The length and mass of the lettuce seedlings were approximately 7 ± 4 cm and 25 ± 5 mg.

Synthesis of Ligand ADIBO-NOTA (6). Unless specified all reagents were purchased from Sigma-Aldrich and used without further purification. The clickable ligand NOTA-ADIBO (**6**) was synthesized following modified literature procedures.[46,47] Briefly: 5-dibenzosuberenone (**1**) (5.0 g, 24.3 mmol) was reacted with *N*-hydroxylamine (1.5 equiv, 2.5 g, 36.4 mmol) in pyridine (Acros, 25 mL) at 80 °C overnight, followed by the acid catalyzed Beckmann rearrangement with polyphosphoric acid (50 mL) at 125 °C. Subsequent reduction of the amide in diethyl ether (Acros, 63 mL) with lithium aluminum hydride ($LiAlH_4$, 2.0 equiv, 1.84 g, 48.6 mmol) afforded amine (**2**) (Scheme 1), which was reacted in *N*,*N*-dimethylformamide (DMF) (EMD, 3 mL) with *N*-[(dimethylamino)-1*H*-1,2,3-triazolo-[4,5-*b*]pyridin-1-ylmethylene]-*N*-methylmethan-aminiumhexafluorophosphate *N*-oxide (HATU, GL Biochem, 2.8 equiv, 250 mg, 0.653 mmol) and

DOI: 10.1021/acs.est.7b03333
Environ. Sci. Technol. XXXX, XXX, XXX−XXX

Scheme 1. Synthesis of ligand ADIBO-NOTA (6)

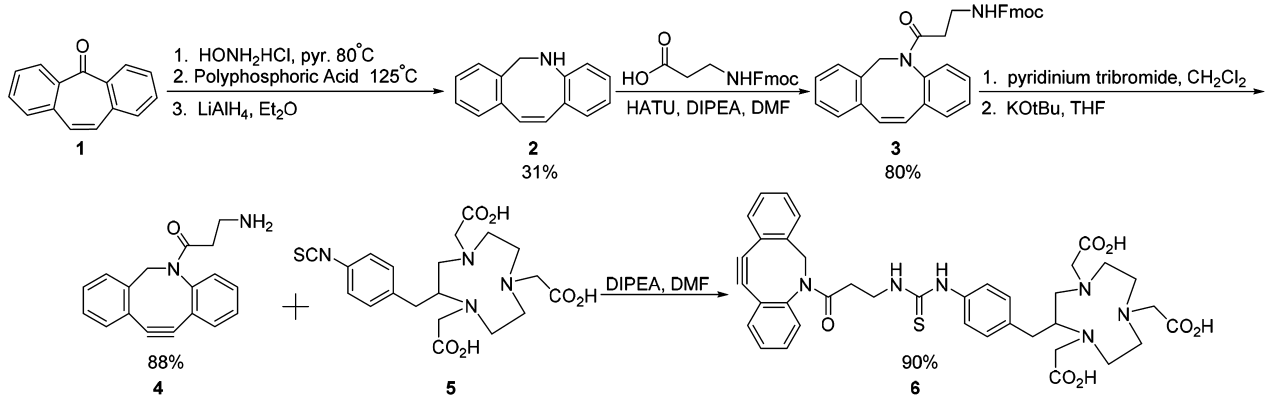

Scheme 2. Radiolabeling and Assembly of [^{64}Cu]-NPs

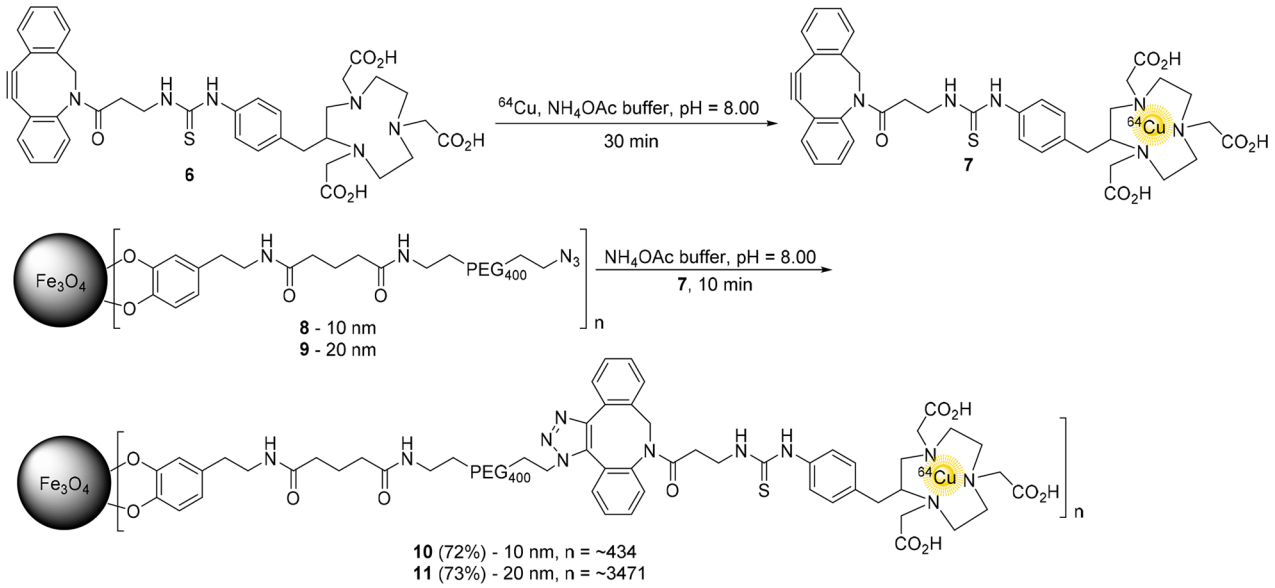

diisopropylethylamine (DIPEA, 6.0 equiv, 250 μL, 1.45 mmol) activated *N*-Fmoc-β-alanine (Novabiochem, 3 equiv, 226 mg, 0.726 mmol) to afford **3**. Compound **3** was *bis*-brominated with pyridinium tribromide and upon double elimination of the bromides with potassium *t*-butoxide (2.5 equiv), strained cyclooctyne (**4**) was produced. Compound **4** was then reacted with 2-(*p*-isothiocyanatobenzyl)-1,4,7-triazacyclononane-*N*,*N*′,*N*″-triacetic acid (**5**) (*p*-SCN-Bn-NOTA, Macrocyclics, 1.0 equiv, 1 mg, 0.0017 mmol) in DMF (100 μL) and DIPEA (5 μL) to afford NOTA-ADIBO (**6**) (1.09 mg, 0.0015 mmol) (Scheme 1). The NOTA-ADIBO ligand (**6**) was purified and analyzed by reversed phase-high performance liquid chromatography (RP-HPLC) jupiter-proteo-C12-column (Phenomenex, 250 mm × 4.6 mm × 4 μm), a mobile phase gradient held for 2 min at 9% acetonitrile in 0.05% trifluoroacetic acid (TFA) aqueous solution and increased to 81% acetonitrile over 30 min at a flow rate of 1.5 mL/min. Purified compound (**6**) was confirmed by mass spectroscopy using electrospray ionization scanning (ESI) for positive ions (Orbitrap, Thermo-Fisher Scientific) (**S2**).

Radiolabeling and Assembly of [^{64}Cu]-NPs. The ADIBO-NOTA (**6**) (400 μL, 1 mg/mL solution in DI water) was used to chelate ^{64}Cu ([^{64}Cu]$CuCl_2$, 4.4−6 mCi, half-life-12.7 h) in an aqueous solution of ammonium acetate (NH_4OAc) at pH = 8.00 (405 μL) for 30 min at room temperature to produce **7**, which was used without further purification. Commercially available azide functionalized catechol-PEG coated Fe_3O_4-NPs (AC Diagnostic, Inc.) (**8**, 10 nm) or (**9**, 20 nm), (1 mg of NP, 200 μL of 5 mg/mL solution) were each reacted with **7** (400 μL, 2.2 mCi) for 10 min at room temperature to afford **10** or **11**, respectively (Scheme 2). Radioactive [^{64}Cu]-NPs (**10** and **11**) were diluted with 600 μL of DI water to a total volume of 1.2 mL and purified using a P6-gel size exclusion spin column (Bio-Rad). Incorporation of ^{64}Cu into **6** and conjugation to NPs (**8** and **9**) was monitored by RP-HPLC (jupiter-proteo-C12-column,Phenomenex, 250 mm × 4.6 mm × 4 μm), a mobile phase gradient held for 2 min at 9% acetonitrile in 0.05% trifluoroacetic acid aqueous solution and increased to 81% acetonitrile over 30 min at a flow rate of 1.5 mL/min. A 10 μL aliquot of each **10** and **11** was diluted with 250 μL of 0.1 M ethylenediaminetetraacetic acid (EDTA) solution and the NPs filtered off via a membrane filter (40 000 molecular weight cut off) by centrifugation (3000 rcf, 4 min (4×)). The filtrate was analyzed by injection onto RP-HPLC as described above. The HPLC-system consisted of a UV-detector (wavelength-220 nm) and a radioactivity detector (PMT) connected in series. Radiochemical purity was also confirmed by thin-layer chromatograpy (TLC) by spotting the EDTA-

DOI: 10.1021/acs.est.7b03333
Environ. Sci. Technol. XXXX, XXX, XXX−XXX

challenged filtrate onto an TLC strip, running with 1.0 M NH_4OAc buffer pH = 8.0, and reading on a radioTLC-scanner (Bioscan 3000)(**S3**).

Characterization of Iron Oxide (Fe_3O_4) NPs. Spherical iron oxide (Fe_3O_4) NPs (**8** and **9**), functionalized with catechol-PEG_{400}-azide ligand were purchased from AC Diagnostic, Inc., (diameter: 10 and 20 nm). The exact size for each batch of NPs (10 nm (**8**) and 20 nm (**9**)) was determined by TEM by finding the mean diameter ($n > 200$). The hydrodynamic diameter was determined by dynamic light scattering (DLS) and the zeta-potential found. This was done for both the azide containing NPs and the functionalized conjugated NPs (**10** and **11**) (**S5**).

TEM Size Determination of NPs. Primary particle size and shape of the Fe_3O_4-NPs was characterized by TEM (Philips CM-12) at 120 kV. Samples were prepared for TEM analysis by placing 10 μL of a stock Fe_3O_4-NP suspension on Formvar film coated Cu grids (Ted Pella) and drying the grids over an incandescent bulb. Mean primary particle size ($n > 200$) for all Fe_3O_4-NP samples (**8**−**11**) of both sizes (10 and 20 nm) was calculated from TEM images using Fiji-software (**S5**).

Dynamic Light Scattering (DLS) Hydrodynamic Size and Zeta-Potential Determination of NPs. Hydrodynamic radius data were collected after sample dispersion (100 mg L^{-1} of Fe_3O_4-NPs (**8**−**11**)) in 1 mM KCl and 1/2 Hoagland's solution by dynamic light scattering at a wavelength of 660 nm using a ZetaPlus (Brookhaven Instruments Corp.). Zeta-potentials were calculated using ZetaPlus software after determining particle electrophoretic mobility (**S5**).

Stability of [^{64}Cu]-NPs. The stability of the [^{64}Cu]-NPs **10** and **11** was assessed over a pH range (5.0, 6.0, 7.0, 8.0, and 9.0) up to 12 h: Radiolabeled [^{64}Cu]-NPs **10** and **11** (30 μL, ∼50 μCi) were incubated in 1 mL of 1.0 M ammonium acetate at the given pH for 4, 8, and 12 h. At each time point for each pH, the [^{64}Cu]-NPs were filtered with a membrane filter (40 000 molecular weight cut off) by centrifugation at 3000 rcf for 4 min (4×). The filtrate was evaluated with a gamma counter (Wizard1470, PerkinElmer) for radioactivity (loss of ^{64}Cu or [^{64}Cu]-ligand) and by HPLC for UV signal (loss of ligand) (**S4**). Additionally, the stability of [^{64}Cu]-NPs (**10** and **11**) was reconfirmed at 15 min, 12 h, and 24 h post exposure to the lettuce seedlings by filtering off the [^{64}Cu]-NPs and examining the filtrate in the same manner (**S4**).

Administration of [^{64}Cu]-NPs to Plants (Time Course Study). Purified [^{64}Cu]-NPs **10** and **11** (20 μL, ∼0.0167 mg NP, per plant) were exposed to lettuce seedlings ($n = 3$) per time point (15 min, 30 min, 1 h, 2 h, 4 h, 12 h, 24 h). The [^{64}Cu]-NPs **10** and **11** suspension was placed into a PCR-tube and diluted up to 350 μL with DI water to give a final concentration of 48 mg L^{-1} of [^{64}Cu]-NP per plant with an activity range between 30 and 34 μCi (32 ± 2 μCi). Plants were then placed into the PCR-tube with only the lower portion of the root exposed to the [^{64}Cu]-NP suspension (lower 2 cm). The experiment was performed at ambient temperature (22 °C) and lighting from incandescent light bulbs. At the end of each time point the plants were removed and the roots were rinsed with DI water (3×) and soaked for 1 h in a solution containing 10%-Triton100X (200 μL, ThermoScientific) and 0.1 M EDTA (200 μL, Sigma-Aldrich) and DI water (200 μL), and rinsed again with DI water (3×); plants were divided into the cotyledons and root portions. Each portion was weighed and radioactivity determined by the gamma counter. Two additional sets of lettuce plants for each set of [^{64}Cu]-NP were given double (40 μL of NP, 96 mg L^{-1}, ∼60 μCi, $n = 3$) and triple (60 μL of NP, 144 mg L^{-1}, ∼90 μCi, $n = 3$) the amount of NPs for a single uptake period of 2 h to examine concentration dependence uptake.

Autoradiography and PET/CT Imaging of [^{64}Cu]-NP in Lettuce. Immediately after gamma-counting and weighing, the plants were exposed to a storage phosphor screen (GE Healthcare) overnight (∼16 h). The screen was read at 50 μm resolution using a Storm 860 phosphorimager (GE Healthcare) and visualized using ImageJ software (Version 1.46r, National Institutes of Health). PET/CT imaging was performed on 3 plants at the 2 h time point. For imaging, the lettuce was placed between two pieces of agarose gel to help with hydration. A static 15 min PET emission scan was acquired on an Inveon-DPET scanner (Siemens Medical Solutions) followed by computed tomography (CT) scan and processed with the Inveon Research Workplace software (Siemens).

Scanning Electron Microscopy (SEM) of Lettuce Roots. After autoradiography the plants were dehydrated in ethanol (1 day) followed by acetone (1 day). Once the radioactivity decayed to background samples were dried under vacuum for 1 day and the adherence of NPs to the surface of the root was examined by scanning electron microscopy (SEM; FEI XL30) at 5 kV, followed by energy dispersive X-ray analysis for elemental analysis.

Transmission Electron Microscopy (TEM) of Lettuce Roots and Cotyledons. To correlate [^{64}Cu]-NP location in the PET/CT and autoradiography images to TEM images, the plant tissue was fixed in Karnovski's fixative, post fixed in 1% osmium tetroxide, dehydrated in cold acetone and infiltrated with Epon/Aradite (Ted Pella). Once the radioactivity decayed to background, the plant samples were cross-sectioned and cut with an Ultra 45 diamond knife (Diatome). The thin sections of fixed, infiltrated plant tissue were then mounted on Formvar film coated Cu grids (Ted Pella) and imaged by TEM (JEOL 2500SE) at 200 kV.

RESULTS

Synthesis, Radiolabeling, and Assembly of NPs. The synthesis of ADIBO-NOTA (**6**) provided an overall yield of 20%, which was comparable to those reported following modified literature protocols[46,47] and was chelated to ^{64}Cu to give **7** with a radiochemical purity of 98% (Scheme 2). The molar activity of radiolabeled ligand **7** was 7297.3 Ci/mol. The attachment of **7** to either **8** or **9** provided approximately the same average radiochemical yield of 72% and 73%, respectively ($n = 18$ spin columns per NP-size, radiochemical yield range 65−80%) of **10** and **11**, respectively, after purification via P6-gel size exclusion spin-column with a specific activity of 2.24 mCi/mg of [^{64}Cu]-NP and a radiochemical purity of >99% for both sized [^{64}Cu]-NP (Scheme 2). Both TLC and RP-HPLC analysis showed no observable UV or radiation signals associated with EDTA-complexed-^{64}Cu (nonchelated ^{64}Cu-ion) and upon "clicking" no observed radioactive ligand was observed (**S3**).

Characterization and Size Determination of NPs. Characterization of the commercially available azide-functionalized NPs **8** and **9** by TEM illustrated that the NPs do not aggregate readily and were spherical in shape. The mean size for the smaller NPs (**8**, 10 nm) was 9 ± 2 nm and for the larger NPs (**9**, 20 nm) was 19 ± 3 nm. NPs (**10** and **11**) showed no change in size by TEM, however, the DLS hydrodynamic radius

DOI: 10.1021/acs.est.7b03333
Environ. Sci. Technol. XXXX, XXX, XXX−XXX

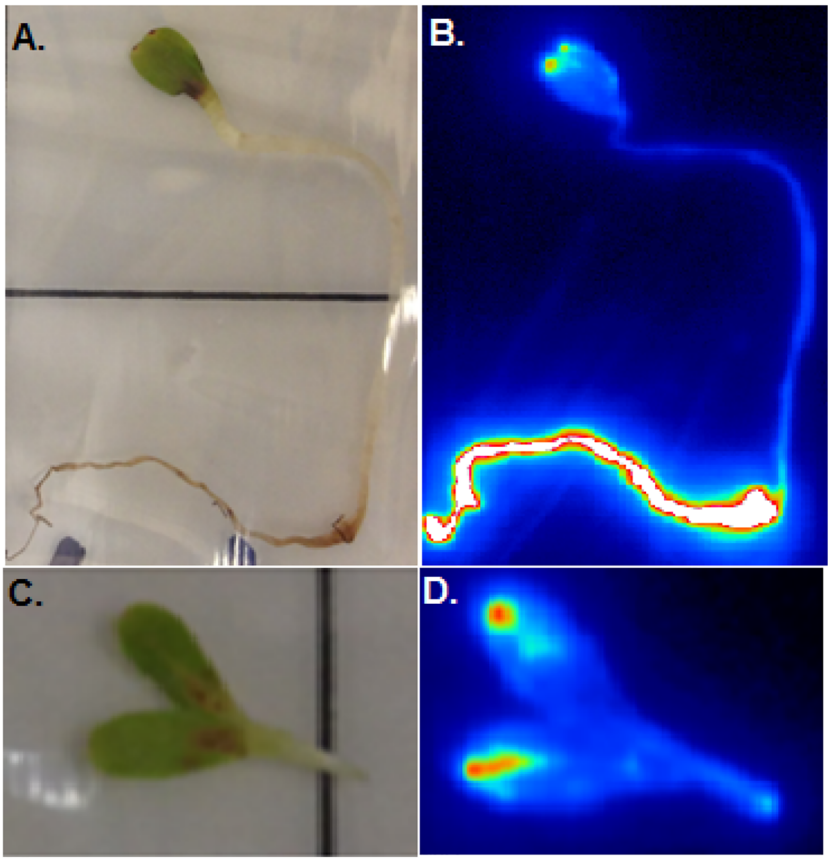

Figure 2. Representative autoradiography image of the lettuce seedling after 2 h exposure to [^{64}Cu]-NPs (**11**). A. Actual photographic image of lettuce seedling. B. Rainbow color scale autoradiography image of the same lettuce seedling. C and D. Representative autoradiography image of the cotyledons removed after [^{64}Cu]-NP (**11**) uptake period (2 h). C. Actual photographic image of lettuce cotyledon. D. Rainbow color scale autoradiography image of lettuce cotyledon. Rainbow color scale: white-highest activity to dark blue-lowest activity.

decreased after "clicking" the ligand, most likely due to added sterics and hydrophobicity providing a smaller hydrodynamic radius. The zeta-potential ranged from −40 to −55 mV, indicating good colloidal dispersion stability (Table S5).

Stability of [^{64}Cu]-NP. RP-HPLC analysis of **10** and **11** after purification via P6-gel size exclusion spin column and after incubation with the plants (15 min, 12 h, and 24 h) showed no free ^{64}Cu or ^{64}Cu-ligand, indicating that once attached, ligand **7** was stable. The conjugated [^{64}Cu]-NP (**10** and **11**) were also stable at all pH's (5−9) up to 12 h by RP-HPLC (**S4**). Furthermore, the NP filtrates up to 24 h exposure to the lettuce, also exhibited only background levels of radiation by gamma-counting and no UV or radiation signal by RP-HPLC analysis (**S4**), signifying no loss of ligand or leaching of ^{64}Cu during the time frame of plant uptake and imaging. TEM was also performed on [^{64}Cu]-NPs (**10** and **11**) after the radioactivity had decayed to background; the size distribution and aggregation properties remained unchanged, indicating a low propensity to dissolute during the plant NP uptake period (**S5**).

Imaging of Lettuce Seedling Uptake of [^{64}Cu]-NP (10 and 11): Autoradiography and PET/CT Imaging. Figures 2 and 3 show a representative autoradiography and PET/CT images demonstrating uptake of [^{64}Cu]-NPs (**10** and **11**) into lettuce seedlings. The appearance of the [^{64}Cu]-NPs in the cotyledons (Figures 2 and 3) in the lettuce seedlings indicate that NPs moved radially across the root tissue submerged in the [^{64}Cu]-NP-suspension, up the root axis (likely traveling

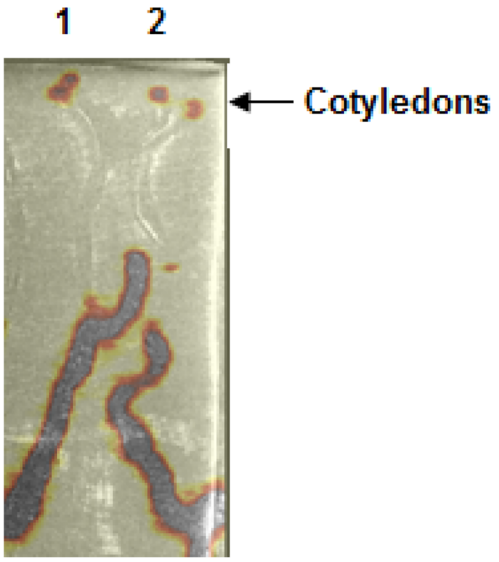

Figure 3. Representative PET/CT image of [^{64}Cu]-NPs (**11**) after a 2 h uptake in two lettuce seedlings. Plants 1 and 2 show [^{64}Cu]-NPs (**11**) in cotyledons.

through early stages of the developing vascular tissue), and into the developing shoot along with water flow. A build-up of [^{64}Cu]-NPs was observed in locations where the root radicle made a bend or turn as seen in some of the autoradiography images (Figures 2 and S9), with the majority of the radioactivity

DOI: 10.1021/acs.est.7b03333
Environ. Sci. Technol. XXXX, XXX, XXX−XXX

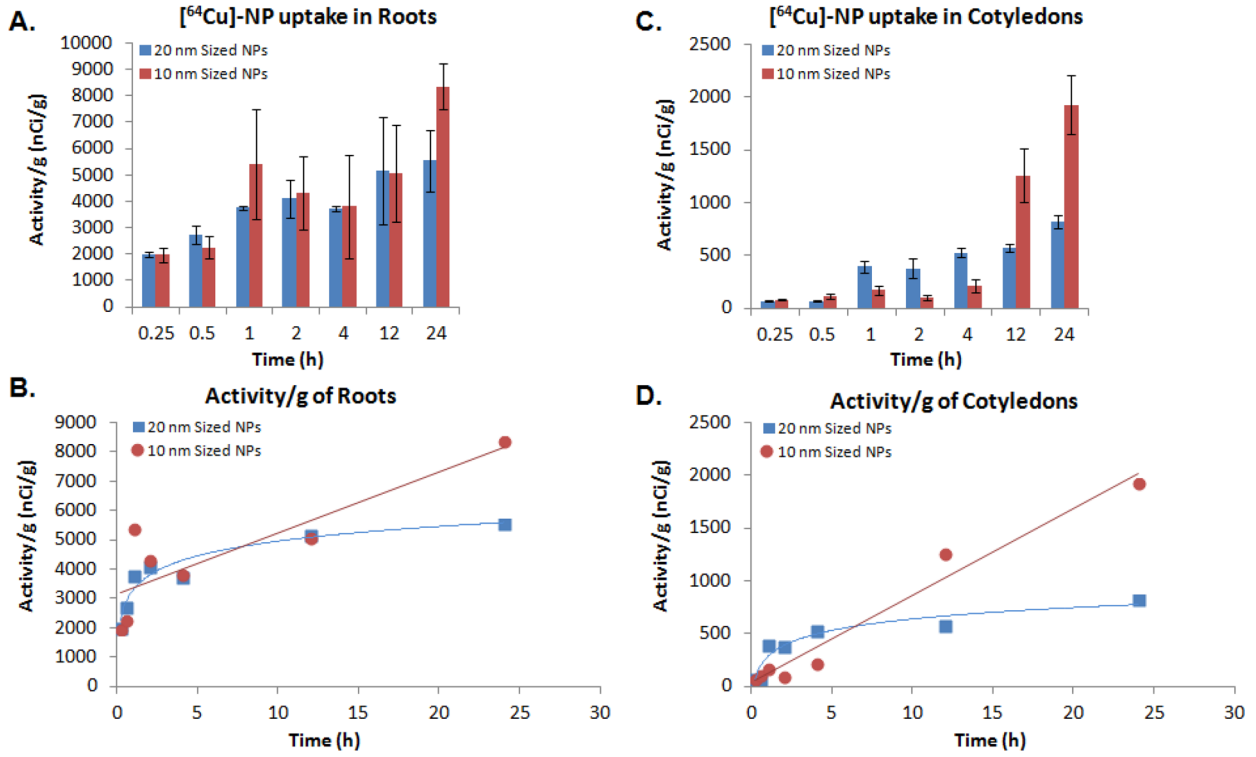

Figure 4. A. Bar graph of [^{64}Cu]-NP uptake in lettuce roots over time (n = 3). B. Decay corrected biodistribution averages (nCi/g) plotted over time to display uptake trend in root (n = 3). C. Bar graph of [^{64}Cu]-NP uptake in lettuce cotyledons over time (n = 3). D. Decay corrected biodistribution averages (nCi/g) plotted over time to display uptake trend in cotyledons (n = 3).

remaining in the lower portion of the root (where it had been submerged) (Figure 2). PET/CT imaging after a 2 h uptake period showed that the [^{64}Cu]-NPs moved readily from the root radicle to the cotyledons and matches the same [^{64}Cu]-NP movement observed by autoradiography (Figure 3).

Plotting the biodistribution averages of radioactivity/gram of lettuce (nCi/g) for both sets of [^{64}Cu]-NPs (**10**, **11**) demonstrated a size-dependent uptake. The average values continually increased over time for the smaller [^{64}Cu]-NPs (10 nm, **10**), while the larger [^{64}Cu]-NPs (20 nm, **11**) biodistribution levelled off after the initial uptake period of 4 h (Figure 4 (B and D), S6). The initial amount of [^{64}Cu]-NPs in the root was higher for the larger [^{64}Cu]-NPs (**11**) being around 1.83 ± 0.11 μg/g (2065 nCi/g) of lettuce (0.25 h), while the small [^{64}Cu]-NPs (**10**) contained 1.50 ± 0.19 μg/g (2043 nCi/g). The initial amount per plant at early time points were not much different for either size, but after 24 h accumulation time, the smaller [^{64}Cu]-NP (**10**) amount was much higher, being 7.56 ± 0.85 μg/g (10276 nCi/g) while the 20 nm [^{64}Cu]-NP (**11**) reached a plateau at approximately 5.7 μg/g (6369 nCi/g). The larger [^{64}Cu]-NPs (**11**) had relatively the same uptake over the 1−12 h time frame with a slightly higher uptake at the 24 h time point with the same trend for **11** in the cotyledons. The smaller [^{64}Cu]-NPs (**10**) had relatively the same quantity of NPs from 1 to 4 h but after 4 h increased linearly. The biodistribution data show that >80% of the [^{64}Cu]-NPs were contained in the root for both sizes over all time points; [^{64}Cu]-NPs **10** showed a range of 4−19% in the cotyledons and [^{64}Cu]-NPs **11** showed 3−14% in the cotyledons (Figures S6). The 24 h time point showed the highest [^{64}Cu]-NP uptake as expected with **10** having 6.15 ± 0.63 μg/g (8350 nCi/g) in the root and 1.42 ± 0.20 μg/g (1927 nCi/g) in the cotyledons and **11** with 4.93 ± 1.03 μg/g (5553 nCi/g) in the root and 0.73 ± 0.05 μg/g (817 nCi/g) in the cotyledons. Interestingly, increasing the concentration (even with higher amounts of radioactivity), had negligible effects on [^{64}Cu]-NPs (**10** or **11**) uptake and accumulation during a 2 h period (~4 μg/g of lettuce)(Figure 5), suggesting a saturable transport or strong bottleneck for movement across the root tissue into the cotyledons.

The biodistribution of radioactivity for each part of the lettuce (root or cotyledons) confirmed that while most the

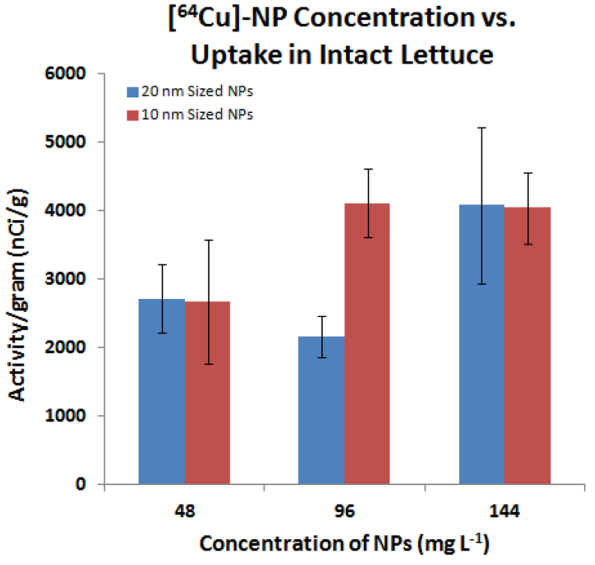

Figure 5. [^{64}Cu]-NP concentration vs uptake in intact lettuce (n = 3) at 2 h.

DOI: 10.1021/acs.est.7b03333
Environ. Sci. Technol. XXXX, XXX, XXX−XXX

radioactivity was in the roots (Figures 4 and S6), some of the [^{64}Cu]-NPs (**10** and **11**) traveled up the root with visible amounts of [^{64}Cu]-NPs being in the cotyledon apex (Figure 2D). The biodistribution data correlated well with the autoradiography and PET/CT images (Figures 2, 3, S6, and S9).

The autoradiography images (Figures 2, S6, and S9) and observed biodistribution suggest that the [^{64}Cu]-NPs were intact during transport as control plants exposed to just radioactive isotope [^{64}Cu]$CuCl_2$ (**S10**) exhibited approximately 4-fold higher activity per gram of plant in the cotyledon and 10-fold more activity per gram in the root radicle. Furthermore, the autoradiography images of the control lettuce seedlings (and additional control duckweed) appear to have a more uniform uptake throughout the plant that correlated to higher amounts of activity, most notably in the cotyledon (**S10**). Additional supporting evidence was obtained from the optically tagged NPs containing a covalently bound fluorescence tag, which also showed the same NP-movement from root to the cotyledon further substantiating intact NP transportation through the lettuce seedlings (**S1**, **S8**).

Plant Uptake of NPs Correlated Imaging: SEM and TEM. Since most of the radioactivity was contained in the root, additional tests were conducted with SEM to verify that this radioactive signal was coming from NPs inside and not adhered to the outer surface of the root (Figure 6A). Unwashed roots exhibited more radioactivity by both autoradiography and gamma counting compared to roots that had been soaked in detergent and EDTA solution prior to imaging and counting of the radioactivity. SEM confirmed that root washing efficiently removed any NPs adhered to the root outer surface (Figure 6A). TEM images of fixed and sectioned lettuce tissue showed the appearance of the [^{64}Cu]-NPs within the plant tissue, indicating intact transport (Figure 6C–F). However, the observed [^{64}Cu]-NPs appeared smaller than those administered for the [^{64}Cu]-NPs (**11**, 20 nm) but exact size determination was difficult due to NP-aggregation.

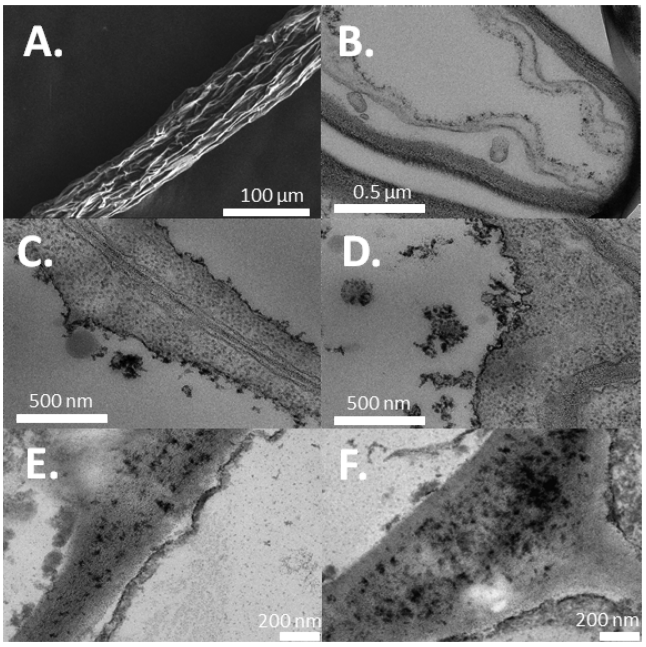

Figure 6. A. Representative SEM image of the lower portion of root exposed to [^{64}Cu]-NP suspension showing no adherence of NPs to the outer surface of the root after washing with EDTA and Triton100X solution. B. Representative TEM image of lettuce not exposed to NPs C. Representative TEM image of lettuce root section after [^{64}Cu]-NP (**10**, 10 nm) exposure. D. Representative TEM image of lettuce cotyledon section after [^{64}Cu]-NP (**10**, 10 nm) exposure. E. Representative TEM image of lettuce root section after [^{64}Cu]-NP (**11**, 20 nm) exposure. F. Representative TEM image of lettuce cotyledon section after [^{64}Cu]-NP (**11**, 20 nm) exposure.

DISCUSSION

To date the uptake, bioaccumulation, biotransformation, and risks of NPs in food crops is not well understood.[8] Most studies on NP uptake in plants have focused on the effects of NPs on plants, and have not focused on the transport or entry of intact-NPs. Several studies concluded that NPs do not gain entry into plants,[22,36−38] while those that do show NP uptake in plants have found the NP amounts to vary widely between 0.05 μg/g and 38983 μg/g of plant.[1,10−16,20,27−30,45] In vivo tracking of NP transport in plants has traditionally relied on destructive analytical techniques to quantify NP-uptake and accumulation, requiring mineralization for metal quantification mostly by ICP.[14−20] These analytical techniques face the challenge of being sensitive enough to reliably measure the small changes in metal concentrations caused by NP-uptake and accumulation within the plant. The extensive range of NP accumulation reported in plants suggests that NP-uptake is dependent on several parameters: (1) quantity of NP administered per plant, (2) plant species, (3) NP-size, (4) NP-composition, and (5) duration of exposure.[1,12,14−18,45] Further complicating the understanding of NP transport and accumulation in plants are the studies that have observed NP-uptake due to dissolution.[14,17−19,33−35] Collectively the variations of parameters in every study on NP transport in plants have made direct comparison and accurate conclusions challenging. Thus, it was our goal to develop a noninvasive visualization approach to track and quantify the distribution of intact radiolabeled [^{64}Cu]-NPs (**10** and **11**) in lettuce seedlings. Using ^{64}Cu-radioactively tagged NPs, we employed a range of complementary noninvasive analytical tools including autoradiography and PET/CT imaging to spatially and temporally visualize and quantify intact-NP uptake and accumulation in plants.

The stability study described demonstrates dissolution of the [^{64}Cu]-NPs did not occur. Ligand effects on NP mobility within the lettuce was minimized by modification of ≤5% of the NP surface with [^{64}Cu]-ADIBO-NOTA (**7**) as to negligibly change the NP surface properties. No ligand detachment or leaching of ^{64}Cu-ion from the NPs within the imaging time frame and at various pHs (**S4**) was observed, by both HPLC and gamma counting analysis, indicating that the radioactive signal in the lettuce seedlings was due to intact [^{64}Cu]-NPs. Additionally, indirect evidence further supported that the observed uptake was from intact [^{64}Cu]-NPs as control lettuce seedlings given only [^{64}Cu]$CuCl_2$ had much higher radioactivity with 4-fold higher concentrations in the cotyledons and 10-fold higher concentrations in the root (Table S10). These control plants also had visibly higher amounts of radioactivity in each part of the plant by autoradiography images (**S10**) suggesting that if the observed radioactivity was due to [^{64}Cu]$CuCl_2$, then the uptake should be much higher. Furthermore, the use of covalently bound optical-tagged NPs (**S1**) also exhibiting high stability and illustrated the same NP movement from the root to the cotyledon (**S8**). Thus, helping to substantiate that NP-uptake and transport to the cotyledon

DOI: 10.1021/acs.est.7b03333
Environ. Sci. Technol. XXXX, XXX, XXX−XXX

was from intact NPs. TEM-sectioning of the plant tissue also helped to corroborate the presence of NPs within the plant tissue (Figure 6). It should be noted that detection of NPs within plant tissue via TEM is challenging,[48] but based on our stability studies of the ^{64}Cu-radiolabeled NPs along with the short exposure time that the observed uptake was attributed to intact [^{64}Cu]-NP transport through the roots and into the cotyledons.

This study has shown that NPs were transported intact into plants and can be tracked noninvasively using a radioactive tag for in vivo imaging by autoradiography and PET/CT and quantification using a gamma counter. This method allows for a highly sensitive method capable of quantifying NP amounts in an individual seedling, a level that would be challenging by the traditional ICP quantification.[1,22,23,26] We found that [^{64}Cu]-NP accumulation in lettuce was size-dependent indicated by the larger [^{64}Cu]-NPs **11** reaching a plateau at a given concentration, while the smaller [^{64}Cu]-NPs **10** increased continually over time (Figure 4). Our study indicates that both sets of [^{64}Cu]-NPs travel intact from the root radicle to the cotyledon (Figures 2 and 3) with the smaller 10 nm [^{64}Cu]-NP (**10**) having a maximum accumulation of 7.56 ± 0.85 μg/g in the whole plant, 6.15 ± 0.63 μg/g in the root, and 1.42 ± 0.20 μg/g in the cotyledons (Figure 4 and Table S6). The larger 20 nm [^{64}Cu]-NPs (**11**) had an accumulation that reached a maximum of 5.66 ± 1.08 μg/g in the whole plant, 4.93 ± 1.03 μg/g in the root, and 0.73 ± 0.05 μg/g in the cotyledon (Figure 4 and Table S6). It is clear from our imaging data, both by autoradiography and PET/CT (Figures 2 and 3) that the [^{64}Cu]-NPs are transported intact from the root to the cotyledons and are present in the lettuce tissue by TEM (Figure 6). However, different accumulation patterns for the cotyledons were observed for the two different sized [^{64}Cu]-NPs (**10** and **11**), while the root and whole plant were similar (Figures 4 and S6). Most of the accumulation for the larger [^{64}Cu]-NPs (**11**, 20 nm) was within the first hour, where cotyledon NP amounts were ∼0.35 ± 0.15 μg/g with the only significant increase after 1 h between the 12 and 24 h time point in which accumulation plateaued at around ∼0.7 μg/g (p-value = 0.004, Student's t test at 95% confidence level) (Figures 4 and S6). The larger [^{64}Cu]-NPs (**11**, 20 nm) also had higher accumulation than the [^{64}Cu]-NPs (**10**, 10 nm) at the early time points up to the 4 h time period. The smaller [^{64}Cu]-NPs (**10**, 10 nm) had ∼8.8 fold increase in cotyledon accumulation from the 4 h time point to the 24 h time point with an increase of ∼1.6 fold between 12 and 24 h time period (Figure 4) appearing to have a linear increase in absorption over time. The differences in cotyledon accumulation between the two sized [^{64}Cu]-NPs maybe linked to NP size effects on the lettuce hydraulic conductivity. Our work suggests that [^{64}Cu]-NPs (**11**) around 20 nm in size appear to clog root cortical cell walls, or pit membrane (or some other bottleneck along the uptake and transport pathway) preventing further uptake, explaining why **11** reaches a plateau, while the smaller [^{64}Cu]-NPs (**10**) continued to increase in amount over time. Initial studies with duckweed also illustrated [^{64}Cu]-NP accumulation in regions of growth and at the node and apex of the cotyledons (Figure S7), suggesting that [^{64}Cu]-NP transport to the cotyledons could occur via the phloem. The TEM images (Figure 6) further shows the appearance of intact NPs in the lettuce tissue within the expected size range for the [^{64}Cu]-NPs (**10**, 10 nm) (Figure 6C, D), but [^{64}Cu]-NPs (**11**, 20 nm) had a size that appeared smaller than those administered; suggesting that the plant may filter larger NPs and has a size-threshold for uptake (Figure 6E, F), which may also explain the clogging phenomenon.[27,28,48] In summary, the combined analysis of the imaging by autoradiography and PET/CT (Figures 2 and 3) and TEM (Figure 6) suggested that both sized [^{64}Cu]-NPs are transported intact from the root to the cotyledons.

The [^{64}Cu]-NP-uptake and accumulation amounts observed within lettuce seedlings were reasonable and comparable to others reports in the literature, reaching the same general conclusions that NP transport and accumulation in plants is species and size dependent.[1,12,16,18,21,23,30] Smaller NPs have been demonstrated to have higher accumulation in plants than larger NPs. For example, Ni-NPs (1, 3, and 9 nm) had very high NP uptake ranging from ∼13 200−38 983 μg/g in mesquite.[45] The amount found in the leaves varied from 400 to 803 μg/g of mesquite with most the NPs remaining in the roots ranging from 12 835 to 38 183 μg/g.[45] Another study using small CeO_2-NPs (7 nm) exhibited NP accumulation ranging from 300 to 6000 μg/g of plant (corn, soy bean, cucumber, tomato, and alfalfa) and indicated that NP accumulation was plant species dependent.[10] NP sizes above active transport ranging from 14 to 40 nm had a large variation in uptake ranging from 0.25 to 3750 μg/g of plant, but typically had accumulation ranging from ∼1−1100 μg/g of plant again with the majority of the NPs contained within the root and with 0.5−183 μg/g in the leaves.[1,15,16,20,27,29] NPs (50 nm), had accumulation in mung bean of 8 μg/g and in wheat of 32 μg/g.[32] When comparing the accumulation of two similarly sized TiO_2-NPs of different crystalline structure [22 nm (rutile) and 25 nm (anatase)] in wheat different accumulation amounts were observed, suggesting size was not the only limiting factor for transportation into a plant.[1]

In another study using radioactive NPs, Zhang et al.[12] generated ^{141}Ce by neutron bombardment of CeO_2NPs synthesized via a precipitation method. The fabrication of [^{141}Ce]CeO_2-NPs could make controlling the size distribution very difficult and the exact size of the radioactive [^{141}Ce]CeO_2-NPs was never determined. In addition, free radioactive ^{141}Ce-metal could dissolute and be transported into the plant, making it appear as if the intact-NPs were in the plant because possible leaching of radioactivity was not explored. We aimed to avoid complications of NP-fabrication in which the exact size distribution during the study could not be determined and to improve upon prior radiolabeling methods, which gave low specific activity (radioactivity/mass of the NP material) of 2.7 μCi/mg of NP.[13] We were able to generate stable radioactive [^{64}Cu]-NPs with high radiochemical purity (>99%) and a specific activity of 2.2 mCi/mg of NP with a tight size distribution (**S5**). Zhang et al.'s work also demonstrated a concentration and size dependence of the [^{141}Ce]CeO_2-NPs on plant accumulation in cucumber.[12] At the lower concentration (20 mg L^{-1}) [^{141}Ce]CeO_2-NPs roots accumulation was ∼370 μg/g for the small 7 nm-NPs and ∼70 μg/g for the 25 nm-NPs. At the highest concentration (200 mg L^{-1}), [^{141}Ce]CeO_2-NP uptake was much higher for both sizes being ∼700 μg/g and ∼500 μg/g of cucumber (7 and 25 nm NPs, respectively).[12] In agreement with our study was that smaller NPs have higher accumulation.

Zhang et al. also noted that accumulation in the leaves was less affected by the size of the [^{141}Ce]CeO_2-NPs with the average uptake in the leaves for the 7 nm-NP being 0.4 μg/g and 0.18 μg/g for the 25 nm-NPs.[12] We observed similar amounts in lettuce cotyledons for the 24 h uptake period with

DOI: 10.1021/acs.est.7b03333
Environ. Sci. Technol. XXXX, XXX, XXX−XXX

the accumulation of **10** being 1.4 μg/g and **11** being 0.7 μg/g. However, the observed accumulation in the cotyledons for [^{64}Cu]-NPs was lower than the amounts observed by Zhang et al.[12] at the very early time points and it was not until the 4 h time point when accumulation amounts in the cotyledons started becoming larger than 0.4 μg/g of lettuce. These uptake differences may be attributed to the use of a different species and/or the NP solution administered had 2.4-times higher concentration (48 mg L^{-1}). Autoradiography images showed [^{141}Ce]CeO_2-NPs movement to the leaves, implying that once NPs entered into the vascular cylinder, they move along with water flow. This was in good agreement with our study. In contrast, we saw no concentration dependence for either sized [^{64}Cu]-NP (**10** or **11**) using 48, 96, and 144 mg L^{-1} over a 2 h period with approximately the same accumulation amount at all concentrations (~4 μg/g of lettuce) (Figure 5). Similarly, another study using CuO-NPs (20−40 nm) administered two concentrations 10 mg L^{-1} and 100 mg L^{-1} for a period of 14 days in maize also observed no concentration dependence.[14]

The use of NPs tagged with radioactivity and tracked by autoradiography and PET/CT has provided a noninvasive analytical tool to spatially visualize and quantify NP uptake and accumulation in plants. We investigated the fate of [^{64}Cu]-NP transport into plants at the largely unexplored early time points, which would prevent dissolution events. Stability studies concluded that the [^{64}Cu]-NPs were stable during the imaging and quantification time frame from 0.25 to 24 h resulting in intact NP-transport into lettuce seedlings. We further demonstrated that the transport of [^{64}Cu]-NPs into lettuce was not concentration dependent but was size dependent with the 20 nm [^{64}Cu]-NPs reaching a plateau with accumulation at ~5.7 μg/g of lettuce and the smaller 10 nm NPs accumulation increasing linearly with the maximum amount at 24 h being ~7.6 μg/g of lettuce. TEM images further substantiated the intact transport of NPs into plants. With the numerous factors that may dictate NP uptake and accumulation, further studies are warranted to fully understand the molecular mechanism of NP transport into plants.

■ ASSOCIATED CONTENT

Supporting Information

The Supporting Information is available free of charge on the ACS Publications website at DOI: 10.1021/acs.est.7b03333.

Details on synthetic compound characterization, click reaction, radiolabeling of NPs, NP characterization, NP stability data, TEM, SEM, and plant section data (PDF)

■ AUTHOR INFORMATION

Corresponding Author

*Phone: 1-916-734-5536; fax: 1-916-734-7572 (J.L.S.).

ORCID

Ryan A. Davis: 0000-0002-0638-870X

Notes

The authors declare no competing financial interest.

■ ACKNOWLEDGMENTS

This work was supported in part by the Office of Science, United States Department of Energy Grant: DE-SC0008385. Additional support is provided by the National Institute of Food and Agriculture, U.S. Department of Agriculture, under grant award number: 2013-67017-21211. We would also like to acknowledge Patricia E. Kysar, Staff Research Associate, Medical Science Electron Microscopy Lab, University of California—Davis and Dr. Fei Guo, Electron Microscopy Facility Director, Electron Imaging Facility, University of California—Davis for SEM and TEM help.

■ REFERENCES

(1) Larue, C.; et al. Accumulation, translocation and impact of TiO_2 nanoparticles in wheat (Triticum aestivum spp.): Influence of diameter and crystal phase. *Sci. Total Environ.* **2012**, *431*, 197−208.

(2) Rodrigues, S. M. T. T; Duarte, A. C.; Pereira, E.; Koopmans, G. F.; Romkens, P. F. A. M.; Trindade, T. A framework to measure the availability of engineered nanoparticles in soils: Trends in soil tests and analytical tools. *TrAC, Trends Anal. Chem.* **2016**, *75*, 129−140.

(3) Aguilera, J. M. Where is the nano in our foods? *J. Agric. Food Chem.* **2014**, *62* (41), 9953−9956.

(4) Magnuson, B. A.; Jonaitis, T. S.; Card, J. W. A brief review of the occurrence, use, and safety of food-related nanomaterials. *J. Food Sci.* **2011**, *76* (6), R126−R133.

(5) Mueller, N. C.; Nowack, B. Exposure modeling of engineered nanoparticles in the environment. *Environ. Sci. Technol.* **2008**, *42* (12), 4447−4453.

(6) Llop, J.; et al. Uptake, biological fate, and toxicity of metal oxide nanoparticles. *Part. Part. Syst. Charact.* **2014**, *31* (1), 24−35.

(7) Ma, X.; et al. Interactions between engineered nanoparticles (ENPs) and plants: Phytotoxicity, uptake and accumulation. *Sci. Total Environ.* **2010**, *408* (16), 3053−3061.

(8) Rico, C. M.; et al. Interaction of nanoparticles with edible plants and their possible implications in the food chain. *J. Agric. Food Chem.* **2011**, *59* (8), 3485−3498.

(9) Gardea-Torresdey, J. L.; Rico, C. M.; White, J. C. Trophic transfer, transformation, and impact of engineered nanomaterials in terrestrial environments. *Environ. Sci. Technol.* **2014**, *48* (5), 2526−2540.

(10) López-Moreno, M. L.; et al. Evidence of the differential biotransformation and genotoxicity of ZnO and CeO_2 nanoparticles on soybean (Glycine max) plants. *Environ. Sci. Technol.* **2010**, *44* (19), 7315−7320.

(11) Baek, Y.-W.; An, Y.-J. Microbial toxicity of metal oxide nanoparticles (CuO, NiO, ZnO, and Sb_2O_3) to Escherichia coli, Bacillus subtilis, and Streptococcus aureus. *Sci. Total Environ.* **2011**, *409* (8), 1603−1608.

(12) Zhang, Z.; et al. Uptake and distribution of ceria nanoparticles in cucumber plants. *Metallomics* **2011**, *3* (8), 816−822.

(13) Stockhofe, K.; Postema, J. M.; Schieferstein, H.; Ross, T. L. Radiolabeling of nanoparticles and polymers for PET imaging. *Pharmaceuticals* **2014**, *7*, 392−418.

(14) Wang, Z.; et al. Xylem- and phloem-based transport of CuO nanoparticles in maize (Zea mays L.). *Environ. Sci. Technol.* **2012**, *46* (8), 4434−4441.

(15) Vittori Antisari, L.; et al. Uptake and translocation of metals and nutrients in tomato grown in soil polluted with metal oxide (CeO_2, Fe_3O_4, SnO_2, TiO_2) or metallic (Ag, Co, Ni) engineered nanoparticles. *Environ. Sci. Pollut. Res.* **2015**, *22* (3), 1841−1853.

(16) Zhang, W.; et al. Uptake and accumulation of bulk and nanosized cerium oxide particles and ionic cerium by radish (Raphanus sativus L.). *J. Agric. Food Chem.* **2015**, *63* (2), 382−390.

(17) Cui, D.; et al. Effect of cerium oxide nanoparticles on asparagus lettuce cultured in an agar medium. *Environ. Sci.: Nano* **2014**, *1* (5), 459−465.

(18) Schwabe, F.; et al. Dissolved Cerium contributes to uptake of Ce in presence of differently sized CeO_2-nanoparticles by three crop plants. *Metallomics* **2015**, *7* (3), 466−477.

(19) Ma, Y.; et al. Phytotoxicity and biotransformation of La_2O_3 nanoparticles in a terrestrial plant cucumber (Cucumis sativus). *Nanotoxicology* **2011**, *5* (4), 743−753.

DOI: 10.1021/acs.est.7b03333
Environ. Sci. Technol. XXXX, XXX, XXX−XXX

(20) Wang, Q.; et al. The impact of cerium oxide nanoparticles on tomato (Solanum lycopersicum L.) and its implications for food safety. *Metallomics* **2012**, *4* (10), 1105−1112.
(21) Miralles, P.; Church, T. L.; Harris, A. T. Toxicity, uptake, and translocation of engineered nanomaterials in vascular plants. *Environ. Sci. Technol.* **2012**, *46* (17), 9224−9239.
(22) Wang, H.; et al. Physiological effects of magnetite (Fe_3O_4) nanoparticles on perennial ryegrass (Lolium perenne L.) and pumpkin (Cucurbita mixta) plants. *Nanotoxicology* **2011**, *5* (1), 30−42.
(23) López-Moreno, M. L.; et al. X-ray absorption spectroscopy (XAS) corroboration of the uptake and storage of CeO_2 nanoparticles and assessment of their differential toxicity in four edible plant species. *J. Agric. Food Chem.* **2010**, *58* (6), 3689−3693.
(24) Nordmann, J.; et al. In vivo analysis of the size- and time-dependent uptake of $NaYF_4$:Yb,Er upconversion nanocrystals by pumpkin seedlings. *J. Mater. Chem. B* **2015**, *3* (1), 144−150.
(25) Hischemöller, A.; et al. Imaging of the uptake of upconversion nanoparticles by plant roots. *J. Biomed. Nanotechnol.* **2009**, *5* (3), 278−284.
(26) He, X.; et al. Quantifying and imaging engineered nanomaterials in vivo: Challenges and techniques. *Small* **2013**, *9* (9−10), 1482−1491.
(27) Lin, D.; Xing, B. Root uptake and phytotoxicity of ZnO nanoparticles. *Environ. Sci. Technol.* **2008**, *42* (15), 5580−5585.
(28) Zhu, H.; et al. Uptake, translocation, and accumulation of manufactured iron oxide nanoparticles by pumpkin plants. *J. Environ. Monit.* **2008**, *10* (6), 713−717.
(29) Zhao, L.; et al. Monitoring the environmental effects of CeO_2 and ZnO nanoparticles through the life cycle of corn (Zea mays) plants and in situ μ-XRF mapping of nutrients in kernels. *Environ. Sci. Technol.* **2015**, *49* (5), 2921−2928.
(30) Stampoulis, D.; Sinha, S. K.; White, J. C. Assay-dependent phytotoxicity of nanoparticles to plants. *Environ. Sci. Technol.* **2009**, *43* (24), 9473−9479.
(31) Lin, S.; et al. Uptake, translocation, and transmission of carbon nanomaterials in rice plants. *Small* **2009**, *5* (10), 1128−1132.
(32) Lee, W.-M.; et al. Toxicity and bioavailability of copper nanoparticles to the terrestrial plants mung bean (Phaseolus radiatus) and wheat (Triticum aestivum): Plant agar test for water-insoluble nanoparticles. *Environ. Toxicol. Chem.* **2008**, *27* (9), 1915−1921.
(33) Koo, Y.; et al. Fluorescence reports intact quantum dot uptake into roots and translocation to cotyledons of Arabidopsis thaliana and subsequent ingestion by insect herbivores. *Environ. Sci. Technol.* **2015**, *49* (1), 626−632.
(34) Ma, Y.; et al. Where does the transformation of precipitated ceria nanoparticles in hydroponic plants take place? *Environ. Sci. Technol.* **2015**, *49* (17), 10667−10674.
(35) Zhang, P.; et al. Species-specific toxicity of ceria nanoparticles to Lactuca plants. *Nanotoxicology* **2015**, *9* (1), 1−8.
(36) Doshi, R.; et al. Nano-aluminum: Transport through sand columns and environmental effects on plants and soil communities. *Environ. Res.* **2008**, *106* (3), 296−303.
(37) Asli, S.; Neumann, P. M. Colloidal suspensions of clay or titanium dioxide nanoparticles can inhibit cotyledon growth and transpiration via physical effects on root water transport. *Plant, Cell Environ.* **2009**, *32* (5), 577−584.
(38) Birbaum, K.; et al. No evidence for cerium dioxide nanoparticle translocation in maize plants. *Environ. Sci. Technol.* **2010**, *44* (22), 8718−8723.
(39) Gardea-Torresdey, J. L.; et al. Formation and growth of Au nanoparticles inside live alfalfa plants. *Nano Lett.* **2002**, *2* (4), 397−401.
(40) Gardea-Torresdey, J. L.; et al. Alfalfa sprouts: A natural source for the synthesis of silver nanoparticles. *Langmuir* **2003**, *19* (4), 1357−1361.
(41) Bali, R.; Siegele, R.; Harris, A. T. Biogenic Pt uptake and nanoparticle formation in Medicago sativa and Brassica juncea. *J. Nanopart. Res.* **2010**, *12* (8), 3087−3095.
(42) Harris, A. T.; Bali, R. On the formation and extent of uptake of silver nanoparticles by live plants. *J. Nanopart. Res.* **2008**, *10* (4), 691−695.
(43) Haverkamp, R. G.; Marshall, A. T. The mechanism of metal nanoparticle formation in plants: Limits on accumulation. *J. Nanopart. Res.* **2009**, *11* (6), 1453−1463.
(44) Wang, Y.; et al. Naturally occurring nanoparticles from Arthrobotrys oligospora as a potential immunostimulatory and antitumor agent. *Adv. Funct. Mater.* **2013**, *23* (17), 2175−2184.
(45) Parsons, J. G.; et al. Toxicity and biotransformation of uncoated and coated nickel hydroxide nanoparticles on mesquite plants. *Environ. Toxicol. Chem.* **2010**, *29* (5), 1146−1154.
(46) Kuzmin, A.; et al. Surface functionalization using catalyst-free azide−alkyne cycloaddition. *Bioconjugate Chem.* **2010**, *21* (11), 2076−2085.
(47) Carpenter, R. D.; Hausner, S. H.; Sutcliffe, J. L. Copper-free click for PET: Rapid 1,3-dipolar cycloadditions with a fluorine-18 cyclooctyne. *ACS Med. Chem. Lett.* **2011**, *2* (12), 885−889.
(48) Taylor, A. F.; Rylott, E. C.; Anderson, C. W. N.; Bruce, N. C. Investigating the toxicity, uptake, nanoparticle formation and genetic response of plants to gold. *PLoS One* **2014**, *9* (4), e93793.

DOI: 10.1021/acs.est.7b03333
Environ. Sci. Technol. XXXX, XXX, XXX−XXX